Manuscript

Photochemical Chain Scissions Enhance Polyethylene Glycol Biodegradability: From Probabilistic Modelling to Experimental Demonstration

Kevin Kleemann[a], Madalina Jaggi[b], Stefano M. Bernasconi[b], Robert Alexander Schmitz[a,e], Glauco Battagliarin[d], Andreas Künkel[d], Carsten Simon[a,e], Kristopher McNeill[a], and Michael Sander[a*]

[a]Institute of Biogeochemistry and Pollutant Dynamics, ETH Zurich, 8092 Zurich, Switzerland
[b]Geological Institute, Department of Earth Sciences, ETH Zurich, 8092, Zurich, Switzerland
[c]current address: Department of Biotechnology, Delft University of Technology, Delft, The Netherlands,
[d]BASF SE, Materials and Formulation Research, Carl-Bosch-Strasse 38, 67056 Ludwigshafen, Germany
[e]current address: Helmholtz-Zentrum für Umweltforschung – UFZ, 04318 Leipzig, Germany

Abstract

Polyethylene glycols (PEGs), a major class of water-soluble polymers (WSPs), are widely used in diverse applications which may lead to their release into the environment. This work investigates the reaction of PEGs with photochemically produced hydroxyl radicals (•OH), an important environmental oxidant, and assesses the effect of reaction-induced molecular weight (MW) decreases on PEG biodegradation dynamics in soil and sediment. Probabilistic kinetic modelling revealed a significant reduction in PEG MW after only a few •OH-induced chain scissions on initial PEG molecules. The simulation results were experimentally validated by reacting ^{13}C-labeled PEGs (average MW = 6200 Da) with photochemically produced •OH, resulting in pronounced shifts in the size distribution of PEGs towards lower MWs with increasing reaction extents. Incubations of the initial non-reacted and three incrementally •OH-reacted PEG mixtures over a 150-day period in sediment and soil demonstrated increasing rates and extents of PEG biodegradation to $^{13}CO_2$ with increasing •OH-reaction extent and thus decreasing PEG average MW. This study underscores the importance of considering the MW distributions of WSPs and their dynamic changes through biotic or abiotic chain scission reactions — showcased herein by reacting PEGs with photochemically produced •OH — in mechanistically understanding WSP biodegradability in natural and engineered receiving environments.

Keywords

Polyethylene glycol (PEG); photochemical degradation; hydroxyl radicals, chain scission; molecular weight distribution; biodegradability; soil, sediment, environmental fate

Synopsis

Indirect photolysis of polyethylene glycols results in lower-molecular weight chain scissions products with enhanced biodegradability in soil and sediment.

Introduction

Polyethylene glycols (PEGs) are a major class of synthetic water-soluble polymers (WSPs) with an annual global production volume of approximately 600 kilotons.[1] In home and personal care products, PEGs act as emulsifiers and moisture carriers.[2,3] In these applications, PEGs are typically diluted in water and are discarded in household wastewater streams. In agricultural formulations, PEGs emulsify and stabilize pesticides and fertilizers, thereby ensuring their efficient application.[4] A common feature of these applications is that PEGs are subject to dissipative release, either to wastewater treatment plants or agricultural soils. The latter may also receive indirect inputs when fertilized with PEG-containing sludge.[5]

Despite these release pathways into natural and engineered systems, the environmental chemistry and fate of PEGs – as well as of WSPs in general – remains poorly studied and understood.[6,7] Besides transport and mobility considerations,[8,9] transformation processes, such as extracellular chain-scission reactions, are of particular relevance. Biodegradation, a process in which microorganisms take up and metabolically convert PEGs into CO_2 and microbial biomass, can be considered the ultimate transformation endpoint. Previous studies have proposed that this microbial utilization of PEGs occurs through end-group specific (i.e., exolytic) oxidation reactions catalyzed by three intracellular enzymes: an alcohol dehydrogenase, which converts the terminal alcohols into aldehydes; an aldehyde dehydrogenase, which oxidizes the aldehydes to carboxylic acids; and, finally, an ether bond-cleaving enzyme (e.g., α-hydroxy acid dehydrogenase), which acts on the carboxylic end groups releasing glyoxylates, thereby shortening the PEG chain by one unit.[10–14] The glyoxylates are then further metabolized to CO_2. Biodegradability is a highly desired property as it prevents PEG molecules from accumulating in the environment and, therefore, constrains the exposure component in environmental risk assessment scenarios, irrespective of potential hazard, which is object of investigation of academic research as well as product safety screening studies.[15–20]

Transformation reactions that beak PEG chains, generating lower molecular weight (MW) molecules, are expected to enhance biodegradability: This is because, first, the number of hydroxyl end groups per unit molecular mass increases while the MW decreases, thereby also increasing the probability of exolytic enzymatic breakdown. Second, uptake rates of PEG molecules across microbial membranes into cells – a prerequisite for intracellular metabolic conversion –are expected to increase with decreasing MW.[21] While the dependency of PEG MW on environmental biodegradation has not yet been systematically studied, the published data support faster biodegradation of PEGs with lower MW. For instance, PEG molecules up to 14600 Da showed complete degradation within 20 days in activated-sludge inoculated freshwater media, while PEG molecules with higher MWs required longer incubations for complete biodegradation (i.e., 60 days for PEGs with a number average molecular weight $\overline{M_n}$ = 57800 Da).[22] Similarly, PEG molecules with average MW of 400 Da biodegraded in agricultural topsoils within 42–71 days [23], while molecules with average MW of 4000 Da biodegraded more slowly (extrapolated biodegradation extent of 50% only after estimated 735 days).[24]

In sunlit aquatic systems, PEGs may react with photochemically produced hydroxyl radicals (•OH), resulting in chain scissions and thus decreasing MW of the PEGs. The rate of this reaction increases with increasing steady-state •OH concentrations ([•OH]ss) in surface water, which are reported to range from 10^{-17} M to 10^{-15} M.[25–30] Major photosensitizers for •OH are nitrate, nitrite, and dissolved organic matter (DOM).[26,31,32] The reaction of PEG with •OH is well-studied for engineered systems as •OH are generated in commonly used water treatment processes such as UV/H_2O_2 treatment and ozonation, which are widely implemented around the world. These studies have shown that PEG chain scissions occur, thereby lowering the average MW and increasing polydispersity index (PDI) of PEGs.[33,34] By contrast, PEG

reactions with environmental •OH and its implications, particularly a hypothesized increase in PEG biodegradability, remain unexplored.

This study systematically assesses the effects of •OH-reaction induced chain scissions on the MW distribution and subsequent biodegradability of PEGs in soil and sediment. Chain scissions of PEGs are hypothesized to enhance biodegradability due to the formed smaller PEG molecules being more readily assimilated and metabolized by microbes. We chose PEG reaction with •OH not only due to its environmental relevance but also as an illustrative example to assess the importance of WSP chain scission reactions on subsequent WSP biodegradation in natural and engineered systems. The hypothesis was tested in a three-step approach: first, we simulated •OH reaction-induced decreases in the average MW of weight-distributed PEG molecules using numerical simulations (Monte Carlo). Second, we experimentally reacted ^{13}C-labelled PEGs (average MW = 6200 Da) with •OH generated by H_2O_2 photoirradiation and tracked the resulting changes in MW distributions of the PEG molecules over time using high-performance liquid chromatography coupled to both a charged aerosol detector and a mass spectrometer (HPLC-CAD-MS). This experimental data was compared to Monte Carlo model predictions. Third, we incubated the initial and three incrementally •OH-reacted PEG molecules in a soil and a sediment and monitored biodegradation dynamics by following the formation of PEG-derived $^{13}CO_2$. This study is the first to link WSP reaction-induced chain scissions to environmental biodegradability and, building on previous studies on structural polymers,[35–38] pioneers the use of stable carbon isotope labeling in WSP environmental fate assessment.

Results and Discussion

PEG chain scissions from reaction with •OH – predictive calculations and numerical modelling.

Modelling decay of number averaged MW of PEG. In a first approach we assumed simple pseudo-first-order reaction kinetics to model the rates of •OH-induced chain scissions in ensembles of MW-distributed PEGs (Eq. 1). As expected, the rate of PEG chain scissions increased with increasing $[\bullet OH]_{SS}$, as shown in **Figure 1a, b** for three theoretical PEG mixtures with initial number-average molecular weight $\overline{M}_n$ of 12, 6, and 3 kDa. For high environmental $[\bullet OH]_{SS}$ of 10^{-15} M (**Figure 1a** - light colors), the average number of scissions per initial PEG chain, $\overline{SiC}$, after one day of reaction was calculated to vary between $\overline{SiC}$= 4 (initial $\overline{M}_n$ = 12 kDa) to 20 (initial $\overline{M}_n$ = 3 kDa). By comparison, for low environmental $[\bullet OH]_{SS}$ of 10^{-17} M (**Figure 1a** - dark colors), ten days of reaction result in $\overline{SiC}$ of 0.5 to 2 for initial $\overline{M}_n$ of 12 and 3 kDa, respectively. In all cases, the chain scissions result in an exponential decrease in $\overline{M}_n$ over time (**Figure 1b**): $\overline{M}_n$ decreases from the initial 12, 6 and 3 kDa to $\overline{M}_n$< 1 kDa within a few days for $[\bullet OH]_{SS} = 10^{-15}$ M and to approximately $\overline{M}_n$= 5, 3.5, and 2.3 kDa within 10 days for $[\bullet OH]_{SS} = 10^{-17}$ M. Residence times of PEGs in sunlit surface waters with elevated $[\bullet OH]_{SS}$ between hours to a few days result in modeled $\overline{SiC}$ from 1 to 8. This result shows that •OH-induced reactions can significantly impact the MW of PEGs in the environment within reasonable timeframes. Therefore, we chose this range of $\overline{SiC}$ values for more detailed kinetic assessments in which we simulated the effect of chain scissions on the entire MW distribution of the PEGs.

Monte Carlo simulations of PEG MW distributions. For illustrative purposes, the results of a single simulation of •OH-induced chain-scission reactions on 20 initial PEG chains are shown in **Figure 1** for $\overline{SiC}$ of 1 (i.e., 20 chain scissions, **panel c**) and 8 (i.e., 160 chain scissions, **panel d**). The 20 initial chains were chosen to be representative of the average MW and the

MW distribution of the ^{13}C-labelled PEG mixture (i.e., 6380 ± 400 Da, average ± standard deviation) used in the experimental part below. For $\overline{SiC}$ = 1 and the given simulation, only 11 of the initial 20 PEG chains reacted with •OH (**Figure 1c**) and thus were part of the '*Intermediate Chains*' pool, while the non-reacting 9 chains were assigned to the '*Final Chains*' pool which defines the MW distribution at the end of the simulation. Each reacting PEG molecule forms two daughter PEG molecules, as shown by two arrows. The formed PEGs were of lower MW and are referred to as 1st generation intermediates because they originated from chain scissions on the initial PEGs. It is important to note that 1st generation intermediates can still be formed after higher-generation products, as chain scissions occur stochastically for each PEG molecule, depending on when they undergo their first reaction event during the simulation. For the shown simulation, 5 solid arrows from the initially reacting 11 PEG molecule point to other '*intermediate*' scission products that subsequently continued to react with •OH. The remaining 22 - 5 = 17 dashed arrows point to PEG products in the '*Final Chains*' pool because in this simulation they did not react further. A total of 9 reaction intermediates formed in the shown simulation up to the third generation (i.e., PEG molecules formed from three previous chain scissions). The simulation was terminated when a total of 20 scissions were reached (i.e., a $\overline{SiC}$ = 1 because these scissions occurred on 20 initial chains, resulting in a total of 40 arrows in **Figure 1c**). The final distribution of simulated PEG chains is shown below the network plot in nr% abundance (i.e., the number of PEG molecules with a given MW over the total number of chains obtained) versus MW. The simulation reveals that many of the initial PEG molecules (approx. 50 nr%) have not reacted at $\overline{SiC}$ = 1 and that those which reacted formed shortened PEG molecules with approximately equal nr% across the entire MW spectrum.

An analogous simulation with $\overline{SiC}$ = 8 as the termination criterion resulted in the reaction of nineteen out of the twenty initial PEG molecules and the formation of scission

products up to the 7th generation, with most products ('*Final Chains*') belonging to the 2nd to 4th scission generations (**Figure 1d**). The most abundant formed PEG molecules had MWs below 2000 Da.

For more reliable statistics and to obtain better-resolved MW distributions of the final pool of PEG molecules, we expanded the simulation by increasing the number of initial PEG molecules to 5000 (but maintaining the MW distribution of 6380 ± 400 Da) and by combining a total of 50 simulation outcomes per $\overline{SiC}$ scenario. We note that the chosen simulation parameters represent a balance between computational feasibility and statistical reliability. For the simulations terminated at $\overline{SiC}$ = 1, a large fraction of the initial PEG molecules did not react, as evidenced from the high abundance and the bell-shaped distribution around the starting average MW of 6380 Da (**Figure 1e**). The simulated final MW distribution of PEG molecules is now expressed in weight percent (wt%) to reflect their actual mass distribution. At the same time, a substantial number of PEGs formed with MWs ranging from 1000 to 5000 Da. Simulations terminated at $\overline{SiC}$ = 2 showed a smaller number of unreacted PEG molecules and an increase in the abundance of formed smaller PEG molecules with chain lengths between 1000 and 6800 Da (with approximately equal abundances of approximately 0.5 wt%). Finally, simulations terminated at $\overline{SiC}$ = 8 resulted in extensive removal of initial PEGs, resulting in PEG molecules with MWs predominantly below 4000 Da.

Figure 1e shows three principal MW-dependent reaction domains: PEGs with high MW - highlighted for the exemplary PEG with MW of 6380 Da as blue vertical line - had a probability of undergoing chain scission was higher than the probability of being formed by chain scission of low abundance higher-MW PEG molecules. As a result, the abundance of high-MW PEG molecules continuously decreased with increasing $\overline{SiC}$s - as shown as blue trace for PEG with MW = 6380 Da in **Figure 1f**. For $\overline{SiC}$ < 1.5, PEG molecules with intermediate

MWs - highlighted for an exemplary MW of 4400 Da in Figure **1e** in purple - had a lower probability of reacting away than of being formed through scissions on higher MW PEGs, thereby resulting in an increase in relative abundance (shown as purple trace for PEG with MW = 4400 Da in **Figure 1f**). Beyond $\overline{SiC}$ = 1.5, however, these PEG molecules had a higher probability of reacting than being formed, resulting in a slow but continuous decrease in their relative abundance with increasing $\overline{SiC}$. Finally, low MW PEG molecules (exemplary MW of 440 Da as green line; **Figure 1e**) had a probability of formation that exceeded the probability of reaction up to the highest simulated $\overline{SiC}$ = 8. Consequently, the abundance of the low MW PEG molecules continuously increases as $\overline{SiC}$ increases (shown for MW= 440 Da in green in **Figure 1f**). We note that the abundance of these low MW PEG molecules would eventually also reach a maximum before decreasing at higher $\overline{SiC}$ values.

Compared to modelling decreases in the $\overline{M_n}$ of the collective PEGs upon reaction with •OH **(Figure 1a, b**), the Monte Carlo simulations offer the advantage of tracking the MW of individual PEGs throughout the reaction. At any simulated $\overline{SiC}$, these individual PEGs can be aggregated to yield an MW distribution over all PEG molecules (**Figures 1c-f**). Information on the MW of individual PEG molecules and their abundance is expected to be critical for the assessment and prediction of PEG biodegradability, given the hypothesized MW-dependence of this process.

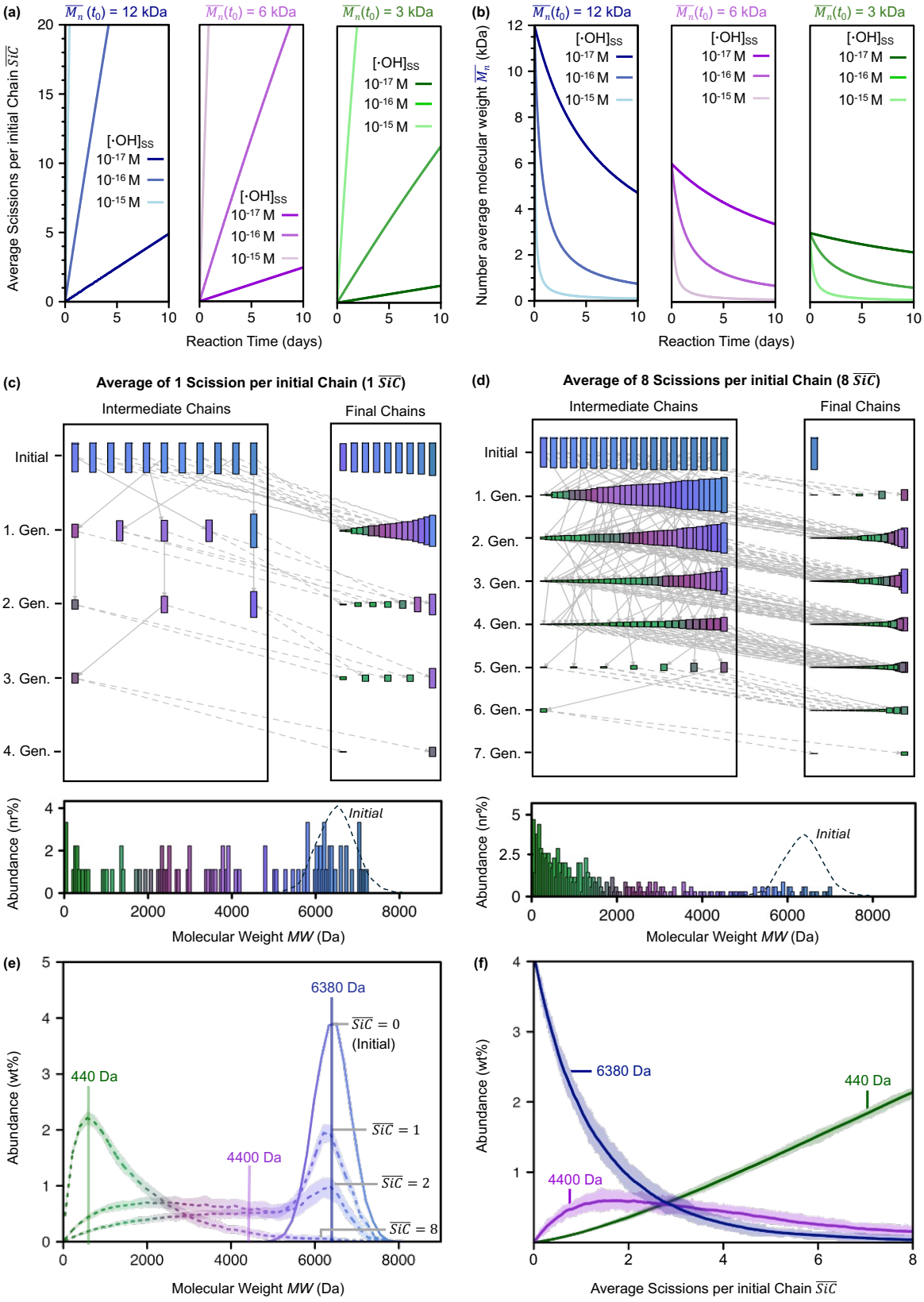

Figure 1. a, b) Pseudo-first order kinetic modelling of the reaction of polyethylene glycol (PEG) with hydroxyl radicals (•OH) results in a linear increase in the average scissions per

initial chain ($\overline{SiC}$) with reaction time (shown up to 10 days; **panel a**), and an exponential decay of the number average molecular weight ($\overline{Mn}$) with reaction time (**panel b**), calculated for $\overline{Mn}(t_0)$ of 12 kDa (blue trace), 6 kDa (purple traces), and 3 kDa (green traces) at three environmental •OH steady-state concentrations of $[•OH]_{SS}$ = 10^{-15} M, 10^{-16} M and 10^{-17} M (shades of the corresponding colour). **c, d**) A reaction network plot illustrating the results of Monte Carlo simulations with 20 initial PEG chains and simulation termination criteria of $\overline{SiC}$ = 1 and 8 in panels **c** and **d**, respectively, with the resulting nr% (i.e., the number of PEG molecules with a given MW over the total number of chains obtained) contributions of individual PEG molecules of given MW plotted below, with the initial MW distribution shown as a dashed line. The PEGs are colour-coded according to MW from high (blues) over medium (purples) to low (greens) MWs. **e, f**) Averaged outputs of 50 Monte Carlo simulations on 5000 initial PEG molecules with an initial MW distribution of 6380 ± 400 Da. Simulation results are depicted as weight percent (wt%) distributions of the MWs of PEG molecules after $\overline{SiC}$ of 1, 2 and 8 (relative to the initial distribution (i.e. $\overline{SiC}$ = 0)). The changes in the wt% contribution of PEG molecules with selected specific MWs (i.e., MW = 6380 Da (blue); MW = 4400 Da (purple); and MW= 440 Da (green) with increasing simulated $\overline{SiC}$ is sg in **panel f**. The 95% confidence intervals of the simulated outputs are shown as shaded areas around the averages in **panels e** and **f**.

PEG chain scissions from reaction with •OH – experimental assessment via UV/H_2O_2 treatment. A solution of ^{13}C-PEG (M_n = 6200 Da, PDI = 1.08, corresponding to an MW distribution of 6380 ± 400 Da) was reacted with •OH produced by UV-light photolysis of H_2O_2 for t_1 = 15 min, t_2 = 30 min, and t_3 = 45 min. Note that ^{13}C-PEGs instead of non-labelled PEGs were chosen due to subsequent $^{13}CO_2$ mineralization studies. An exemplary HPLC-CAD chromatogram of PEG molecules in solution after t_1 = 15 min of reaction is shown in **Figure 2a**. The entire set of chromatograms including the initial PEG solution (t_0= 0 min; no photolysis) and the three reaction times t_1, t_2, and t_3 are provided in section **S2** (Supplementary Information). Individual PEG molecules were well separated over a large MW range from 2000 to 6400 Da. Over this MW range, assignment of the peaks in the chromatogram to specific PEG molecules of defined MW was based on simultaneous analysis of the column effluent by HR-MS (**Figure 2a**). The elugrams for three targeted ions (m/z of 1758, 1873, 1988 (all z= 2), corresponding to PEG molecules with n= 76, 81, and 86 repeat units (with MW of the $^{13}C_2$-

monomeric units of 46.05 Da)) are shown in **Figure 2b**. The exact masses were assigned based on the corresponding HR-MS spectra (**Figure 2c**). Separation of individual PEG molecules decreased at higher loadings onto the HPLC column, as was the case for PEGs with MW > 5000 Da and MW < 3000 Da for experimental solutions from t_1. As a result, integral calculations over these MW regions showed higher uncertainties (as further discussed below). Separation was insufficient for PEGs with MWs below ~2000 Da (filled green peak area below 20 mins of elution in **Figure 2a**) and above ~6400 Da (filled purple peak starting above 810 mins of elution in **Figure 2a**).

The initial ^{13}C-PEG molecules in the unreacted solution had a relatively broad MW distribution starting from approximately 4000 Da, with a maximum in abundance around 6200 Da (t_0 line in **Figure 2d**). Integration of the CAD peaks in the t_0-sample chromatogram revealed that approximately 50 wt% of the PEG molecules were below the $\overline{M_n}$ = 6200 Da given by the supplier (Polymer Source Inc., Dorval, QC, Canada), indicating a symmetric MW distribution (**Figure 2e**). As expected, reaction of the initial PEG molecules with •OH formed lower MW PEGs. With increasing reaction time from t_1 to t_3, the MW distribution of PEG molecules became more uniform across the MW range from 2000 to 6400 Da (**Figure 2d**). Further, the abundance of PEG molecules with MW < 2000 Da (ordinate intercepts in **Figure 2e**; obtained by integration of the poorly resolved early peak in the sample chromatogram (**Figure 2a**)) increased from 0 wt% for t_0, to 18, 25, and 49 wt% for t_1, t_2, and t_3, respectively, while the abundance of the high MW fraction > 6400 Da decreased from ca. 50 wt% for t_0 to 30, 25, and 20 wt% for t_1, t_2, and t_3, respectively. The abundance of the latter may have been slightly overestimated as the MS spectra revealed that also few small PEGs eluted in the high MW elution time region of the chromatogram (labelled > 6400 Da in **Figure 2a**). At the same time, the summed integrals of all peaks in the sample chromatograms, including the poorly resolved peaks for MW < 2000 Da and > 6400 Da (**Figure 2a**), yielded similar values for all four tested

solutions, indicating that reaction of PEG with •OH had caused little (if any) photo-mineralization in the current setup.

Fitting the Monte Carlo simulation with increments of 0.1 SiC (parameters see above, dashed lines) to the measured cumulative MW distribution data (solid lines) resulted in estimated $\overline{SiC}$ of 1.2, 2.1 and 3.9 for t_1, t_2, and t_3, respectively (**Figure 2d)**. The good agreement between the fits and the experimental data suggests that the reaction-limited and diffusion-limited regimes in the cutting kinetics of the PEG chains by •OH assumed in the simulations are in good agreement with the experimental observations. The slightly higher fitted (dashed line) than experimental (solid line) abundances of PEG scission products with MW > 4500 Da may reflect that the concentrations of PEGs in this MW range were low, particularly at t_3, and may have approached the limit of quantification of the HPLC-CAD method. The fitting also revealed that the experimental design resulted in realistic environmental scenarios (i.e., $\overline{SiC}$ from 1 to 4), in good agreement with $\overline{SiC}$ values anticipated for environmentally realistic steady state •OH concentrations ($[•OH]_{SS} = 10^{-16}$ M) and residence times between 12 hours and 3 days (**Figure 1a**).

MS spectra contained peaks with a positive mass offset of 16 Da relative to the original ^{13}C-PEG molecular masses, indicating the presence of PEG reaction products in which a hydrogen was replace by a hydroxyl group. Furthermore, the intensities of peaks with a mass difference of -2 Da increased with increasing reaction time, consistent with end-group aldehyde formation on some products. These chemical changes were confirmed by collecting ^{13}C-NMR spectra on aliquots of the initial and the three irradiated PEG solutions (^{13}C-NMR spectra are provided in section **S2**; Supplementary Information). The ^{13}C-NMR NMR spectra supported not only the formation of end-group aldehydes and acids, but also the formation of some in-chain ester bonds or low MW products, albeit at low abundance (e.g., formaldehyde at a

chemical shift of 82 ppm or acids at 164 ppm). Both the HR-MS and ^{13}C-NMR data are in agreement with the mechanisms and product formation previously proposed when reacting PEG with •OH.[33,39,40]

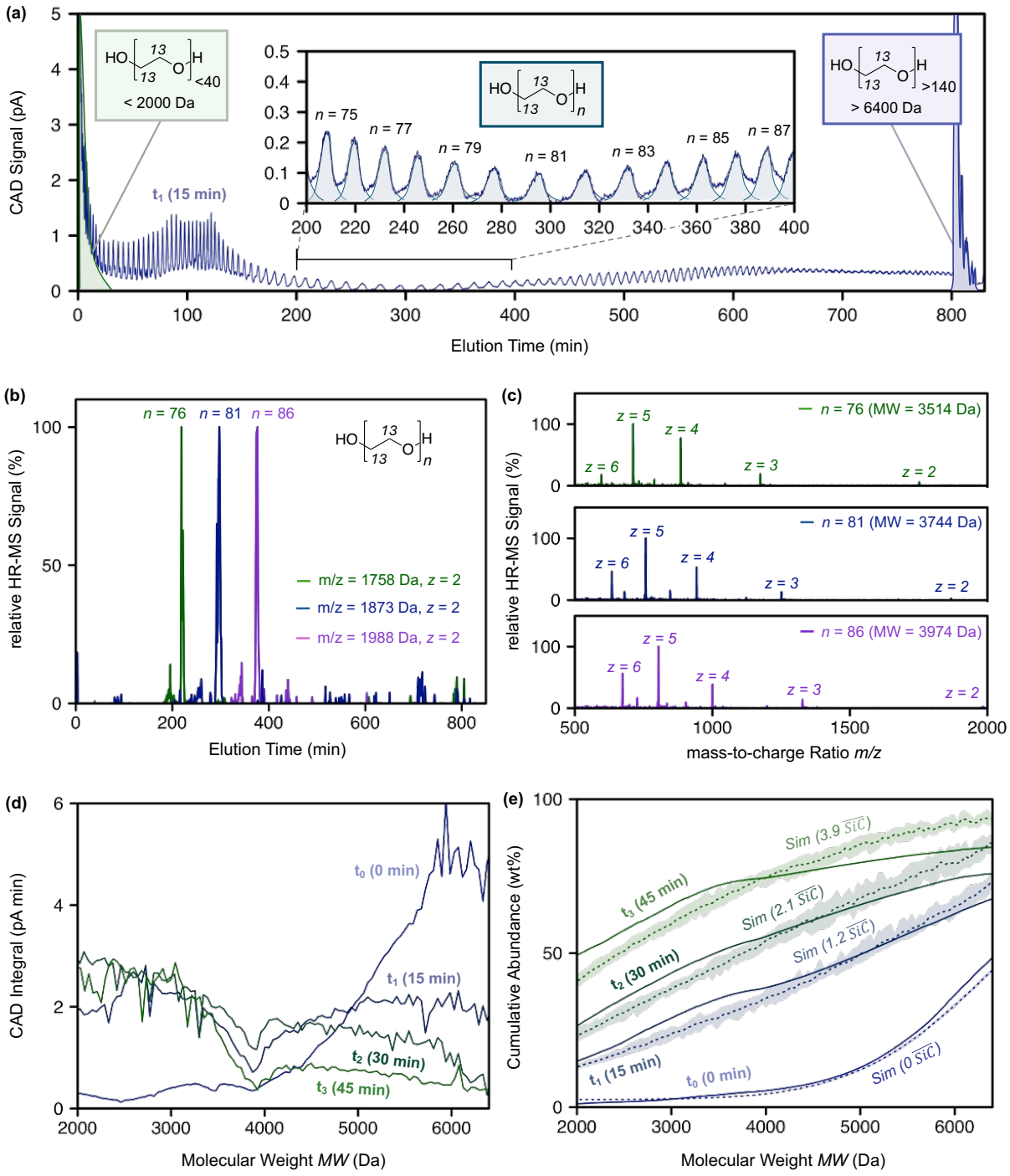

Figure 2. a) Chromatogram of the ^{13}C-polyethylene glycol (PEG)-containing solution after a reaction time of t_1 = 15 min with hydroxyl radicals (•OH), as analysed by high pressure liquid chromatography coupled to charged aerosol detection (HPLC-CAD). The retention time

window from 200 to 400 min is shown in the insert, highlighting the well-separated peaks for individual PEG molecules with repeat unit numbers, n, from n = 75 (corresponding to a molecular weight (MW) of 3124 Da) to n= 87 (MW = 3652 Da). Peak integrals are given in light blue in the insert). PEG molecules with MWs below 2000 Da (green peak) and above 6400 Da (purple peak) are highlighted. The peaks detected by CAD were assigned to PEG molecules with specific MWs by parallel high resolution mass spectrometry (HR-MS) detection (see **panels b** and **c** and all spectra in section **S2**, Supplementary Information). **b)** HR-MS signal chromatogram followed for three individual ion traces with mass-to-charge ratios of m/z = 1758 (green trace), 1873 Da (blue trace), and 1988 Da (purple trace), with intensities normalized to the highest peaks. These peaks correspond to the elution of PEG molecules with n = 76, 81, and 86 repeat units (all z = 2). **c)** Mass spectra of the eluting peaks with highest signal intensity in **panel b)**, showing the mass of the eluted PEG at different molecular charges z. **d)** Integrals of CAD peaks for each identified PEG with a defined MW over the MW range from 2000 to 6400 Da for the unreacted solution (i.e., t_0 = 0 min) and for the solutions reacted for t_1 = 15 min, t_2 = 30 min, and t_3 = 45 min. **e)** Cumulative sum of CAD peak integrals normalized to the total area of the sum over all CAD peaks (solid lines), including the poorly resolved features at < 2000 Da and > 6400 Da, representing the cumulative abundance of PEG molecules versus MW. The dashed lines and corresponding shades represent the best fits of the Monte Carlo simulation and their 95% confidence intervals to the experimental data.

PEG chain scissions from reaction with •OH – effect on PEG biodegradability in soil and sediment. The formation of PEG molecules with lower MW (including the above-mentioned oxidized PEG variants) due to •OH-induced chain scissions is hypothesized to result in enhanced biodegradability. This hypothesis was tested by incubating aliquots of the unreacted PEG solution (i.e., t_0 = 0 min) and the three reacted PEG solutions (i.e., UV/H_2O_2 treatmemt times *t*: t_1 = 15 min, t_2 = 30 min, and t_3 = 45 min of reaction) in triplicate in a reference soil and sediment. The use of ^{13}C-labelled PEGs enabled the selective quantification of PEG mineralization to $^{13}CO_2$ (i.e., $^{13}C_{Mineralized}$) over the course of the incubations, as well as the total non-mineralized PEG-added ^{13}C (i.e., $^{13}C_{Non\text{-}Mineralized}$) that remained in the soil and sediment at the end of the incubations.

Sediment incubations. Incubation of the unreacted ^{13}C-PEG solution (i.e., t_0) in Rotsee sediment resulted in low initial mineralization rates. These rates increased over time and peaked at a maximum rate of 0.97 ± 0.32 %^{13}C h^{-1} at around 6 days of incubation (**Figure 3a**;

rates shown for the first 20 days of incubation). Thereafter, mineralization rates continuously decreased to low values around 0.002 %^{13}C h^{-1} at 20 days. Time-integration of the mineralization rates yielded the cumulative mineralization extent of $^{13}C_{Mineralized}$ = 66 ± 3 % of the initial PEGs at the end of the incubation after 150 days (**Figure 3b**; t_0). Similar to the incubation of unreacted solutions, incubation of the three reacted PEG solutions showed maxima in mineralization rates at around 6 days of incubation with values varying between 0.8 and 1 % ^{13}C h^{-1}. However, incubations of the three reacted PEG solutions showed an additional maximum in mineralization rates at 2 days of incubation with rates increasing from 0.1 % ^{13}C h^{-1} for t_1 to approximately 0.3 %^{13}C h^{-1} for t_3. These peaks in mineralization rates likely corresponded to microbial utilization of low MW PEG molecules formed through reaction with •OH, with cumulative mineralization extents after 3 days of incubation increasing from 4 % (t_1), to 7 % (t_2) and 9 % (t_3). Furthermore, the final mineralization extents also increased from $^{13}C_{Mineralized}$ = 71 ± 0.5 % for t_1, to 76 ± 4.1 % for t_2, and 79 ± 3 % for t_3 of the ^{13}C added, all of which were higher than the $^{13}C_{Mineralized}$ = 66 ± 3 % for t_0 (**Figure 3b**). After terminating the incubations, sediment aliquots were analyzed by EA-IRMS for quantification of $^{13}C_{Non\text{-}Mineralized}$. For all four sediment samples, the mass balance on PEG-added ^{13}C was complete, as $^{13}C_{Non\text{-}Mineralized}$ and $^{13}C_{Mineralized}$ added up to between 96 ± 1 % and 98 ± 2 % of the total PEG-^{13}C initially added into the incubation flasks (**Figure 3e**). Closing the mass balance is a unique feature of using ^{13}C-labelled polymers.

Soil incubations. Incubation of the unreacted PEGs (i.e., t_0 solution) resulted in a small maximum in mineralization rates of ~ 0.035 %^{13}C h^{-1} after 20 hours, after which mineralization rates decreased to low and approximately constant values of ~ 0.0005 %^{13}C h^{-1} over the rest of the incubation (**Figure 3c**). The low final $^{13}C_{Mineralized}$ = 1.25 % after 150 days of incubation (**Figure 3d**) revealed that the PEG molecules with MWs around 6200 Da did not readily biodegrade in this soil. Incubation of PEGs from the reacted solutions showed higher initial

normalized mineralisation rates that reached global maxima also after approximately 20 hours of incubation. The mineralization rates increased with increasing •OH reaction time to values of 0.17 $\%^{13}C\ h^{-1}$ for the most reacted PEGs (i.e., t_3 solution). After approximately 4 days of incubation, the •OH-reacted PEGs showed a second, smaller maximum in normalized mineralization rates which increased from 0.012 $\%^{13}C\ h^{-1}$ for the t_1 sample to approximately 0.024 $\%^{13}C\ h^{-1}$ for the t_3 sample. At this point, cumulative mineralization extents reached 4, 6, and 8 % for the t_1, t_2, and t_3 samples, respectively, while it was below 0.1 % for t_0 sample (**Figure 3d**). The mineralization rate subsequently decreased for all reacted PEGs to values between ~ 0.002 $\%^{13}C\ h^{-1}$ (t_1 solution) and 0.007 $\%^{13}C\ h^{-1}$ (t_3 solution). Distinct increases in the mineralization extents of treated PEGs were observed at around 40 days of incubation resulted from wetting of the soil to re-adjust its water content (**Figure 3d**) and are further discussed below. Final mineralization extents after 150 days of incubation increased with increasing reaction of PEGs with •OH from $^{13}C_{Mineralized} = 20 \pm 0.8$, to 34 ± 3.2, and 45 ± 0.3 % for the t_1, t_2 and t_3 samples, respectively (**Figure 3d**). Given that $^{13}CO_2$ was still formed when incubations were terminated, higher final extents would have been obtained if the soil incubations had been continued beyond 150 days. Quantification of $^{13}C_{Non\text{-}Mineralized}$ in the soils closed mass balances on total added ^{13}C for all soil incubations (i.e., mass balances between 97 ± 2 % and 104 ± 4 % of ^{13}C added; **Figure 3f**).

Comparison of PEG biodegradation in sediment and soil. In both sediment and soil, the rates and final extents of PEG mineralization to $^{13}CO_2$ increased with increasing •OH reaction time, confirming the hypothesis that PEG chain scissions under formation of smaller PEG molecules increase PEG biodegradability – and , thereby, that considering PEG reaction with •OH is sunlit environments is important when estimating PEG biodegradation half-lives. The increase in biodegradation of PEG upon reaction with •OH was less pronounced in the sediment for which already the unreacted PEGs attained high mineralization extents.

Conversely, since the unreacted PEGs did not biodegrade in soils, the effect of forming biodegradable PEG molecules with lower MW from •OH-reaction induced chain scissions was much more pronounced. This finding suggests a much stronger MW dependence of PEG biodegradation in soils than sediments – and that PEG chain scission reactions may lift biodegradation restrictions in soils. In fact, the final mineralization extents closely match the fractions of PEGs with MW < 2000 Da of 21, 35, and 55 wt% for the t_1, t_2, and t_3 samples, respectively, as determined by HPLC-CAD. This finding suggests an upper limit for PEG biodegradation in soils under the given conditions is between 2000 and 2500 Da.

The nature of the non-mineralized PEG-added ^{13}C in both sediment and soil incubations was not identified but may have included both residual PEG molecules with comparatively high MW as well as PEG-derived ^{13}C incorporated into sediment microbial biomass. The latter seems plausible for sediment incubations given that even the non-reacted PEGs underwent extensive mineralization. In this case, the slow and continuous $^{13}CO_2$ formation in the sediment during later stages of the incubation would reflect the slow turnover of microbial biomass containing PEG-derived ^{13}C. While biomass incorporation of PEG-^{13}C may have also occurred during soil biodegradation, the $^{13}C_{Non\text{-}Mineralized}$ for the soil incubations were too high to have resulted exclusively from biomass incorporation: maximum carbon use efficiencies of soil microorganisms of around 0.5 have been reported, implying that at most 50 % of the metabolized carbon can become biomass-incorporated.[41] It therefore is likely that a significant fraction of $^{13}C_{Non\text{-}Mineralized}$ corresponded too PEG molecules with MWs too high to be microbially accessible.

The restricted biodegradation of PEGs with high MW in the soil as compared to the sediment may have two general explanations. First, it is conceivable that microorganisms capable of metabolizing PEGs were more abundant and/or active in the sediment than the soil. However, this explanation is disfavored by the finding that PEGs with low MW were readily

mineralized in the soil, demonstrating that it contained active microorganisms capable of enzymatically metabolizing PEGs.

The second and more likely explanation is that the bioavailability of larger PEG molecules was lower in the soil than the sediment. Limited bioavailability in soils may have resulted from both spatial separation between the PEG molecules and the cells and, in case of close contact, slow uptake into the cell of soil microorganisms. The soil incubations were static (i.e., non-stirred) and conducted under unsaturated conditions (i.e., 50% of the soil WHC) – likely resulting in low rates at which spatial separation between PEGs and cells were overcome. Adsorption of PEGs to soil particles may have further lowered bioavailability. Conversely, sediment incubations were fully water-saturated and continuously stirred and therefore likely resulted in high transfer rates of PEG molecules to cell surfaces (and less adsorption of PEGs due to competitive displacement from particle surfaces by water). Furthermore, it is possible that differences in the cell wall architecture and membrane rigidities between soil and sediment microorganisms resulted in a more stringent MW-cutoff for microbial uptake in soils.[42,43] Further work is needed to elucidate uptake mechanisms, including diffusion of sufficiently low MW PEGs across membranes, potential partial uptake of larger PEG molecules into microbial cells with one chain end to then undergo intracellular exolytic processing – followed by continuous gradual uptake and processing of the remainder of the PEG chain, and endocytosis.[21,44] Differences in the uptake pathways may control the MW at which PEG molecules undergo fast intracellular processing.

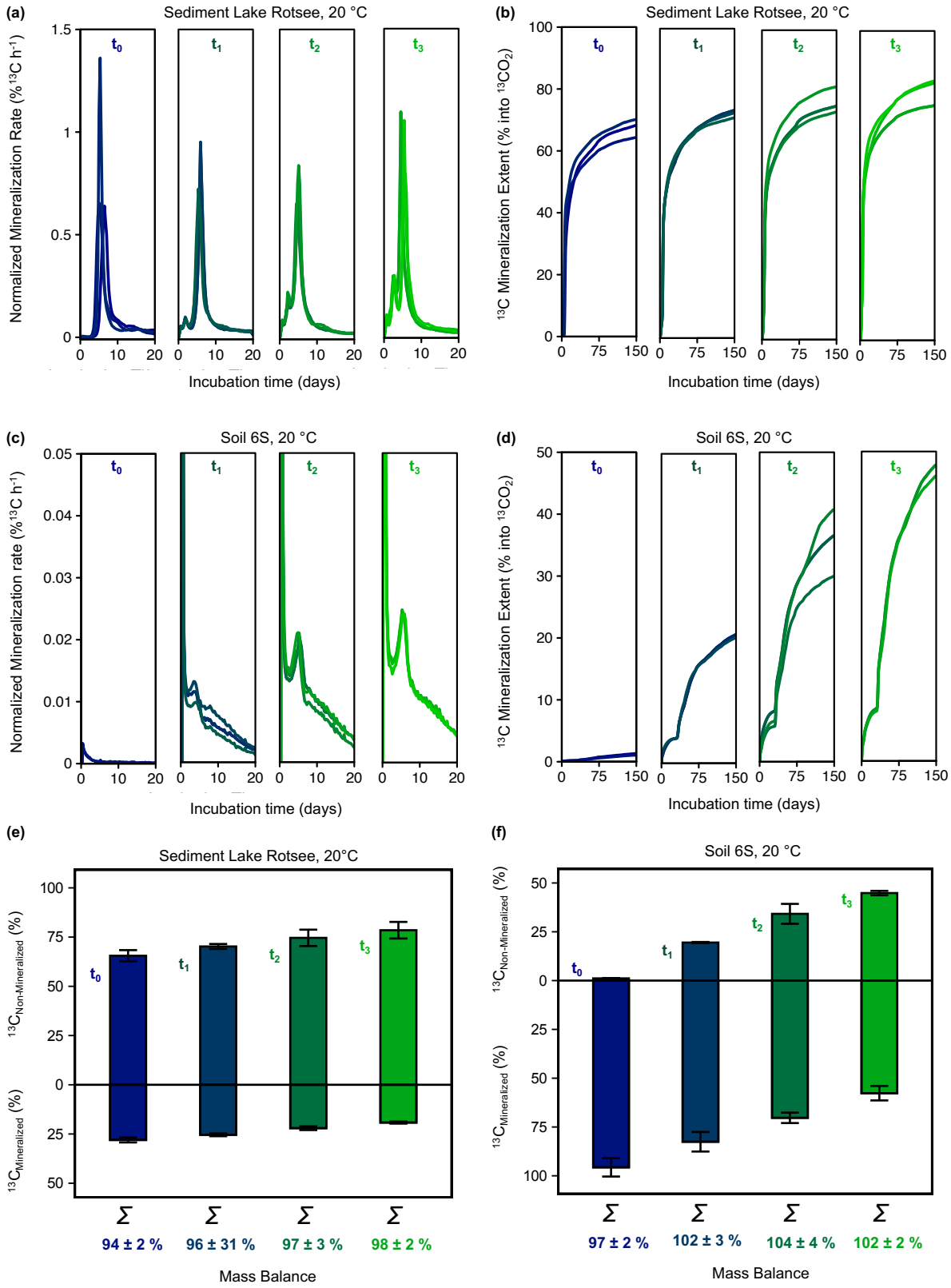

Figure 3. Sediment and soil biodegradation of ^{13}C-labelled polyethylene glycol (PEG) molecules that either were unreacted (i.e., t_0 = 0 mins; dark blue; with a molecular weight (MW) distribution of 6380 ± 400 Da) or reacted with •OH for increasing durations of t_1 = 15 mins (dark cyan), t_2 = 30 mins (dark green), and t_3 = 45 mins (light green) and thus containing increasing amounts of PEG molecules with low MW. **(a, c)** Normalized ^{13}C-based

mineralization rates of ^{13}C-PEG to $^{13}CO_2$ and **(b, d)** the corresponding cumulative mineralization extents expressed as CO_2-^{13}C formed in percent of initially added PEG-^{13}C. Incubations in sediment of lake Rotsee (water-dispersed slurries, continuously stirred) and soil LUFA 6S (unsaturated pore water conditions, static) were run at 20°C under oxic conditions. Non-mineralized PEG-added ^{13}C that remained in the sediment of lake Rotsee **(e)** and soil LUFA 6S **(f)** at the end of the incubations (i.e., $^{13}C_{Non\text{-}Mineralized}$; in ^{13}C in percent of total added PEG-^{13}C) plotted versus cumulative mineralization extents at the end of the incubations (i.e., $^{13}C_{Mineralized}$; as CO_2-^{13}C in percent of total added PEG-^{13}C). Mass balances on PEG-added ^{13}C (i.e., $^{3}C_{Mineralized}$ + $^{13}C_{Non\text{-}Mineralized}$ in % of total added PEG-^{13}C) were closed as shown by numbers close to 100% below the panels. Incubations were run in triplicates, (doublicates for Soil 6S; t_0, dark blue due to limited incubator space and t_3 light green due to flushing issues in the incubator) individual triplicate data are shown in panels (**a-d**), while averages and standard deviations (error bars) are shown in panels **e** and paned **f**.

Environmental Implications

This study underscores the critical role of photochemically produced •OH in the environmental fate of PEGs, a key class of WSPs. Chain scissions in PEGs that result from reaction with •OH are expected to occur widely in sunlit surface waters (e.g., lakes, rivers, and agricultural ditches, where PEG inputs may originate from effluents of wastewater treatment plants, and agricultural runoff) as well as on wet, sunlit surfaces (e.g., plant leaves or soil minerals) that receive PEGs from agricultural formulations. Chain scissions cause a shift in the MW distribution of PEGs toward smaller molecules, which are subsequently biodegraded much more rapidly and extensively in soils and sediments than the higher-MW parent molecules. This underscores that the environmental stability and (bio)degradation rates of PEGs largely depend on their specific MW.

Beyond PEGs, this work demonstrates that robust environmental fate assessments of WSPs, particularly when biodegradation is included as the ultimate transformation endpoint, must account for polymer chain scission reactions and the resulting changes in the MW distribution of WSPs. The probabilistic Monte Carlo simulation model developed and experimentally validated in this study provides a versatile tool to predict chain scissions in WSPs and their impacts on MW distribution. This model can be adapted for WSPs undergoing position-specific

chain scission reactions, such as those driven by abiotic or enzymatic hydrolysis of specific bonds in the polymer backbone.

Our findings emphasize the importance of a MW-specific approach to evaluating the fate and stability of WSPs in both natural and engineered systems. Low-MW molecules within a given WSP class may be readily taken up and metabolized by microorganisms, rendering them (readily) biodegradable, while high-MW molecules with identical chemistry may be stable due to limited microbial availability rather than 'chemical recalcitrance' to metabolic processing inside the cell. To advance the current state of knowledge, future work should systematically investigate MW-dependent WSP biodegradation across terrestrial and aquatic environments and elucidate the underlying mechanisms driving potential differences. Ultimately, accurate characterization of MW distributions is essential for advancing biodegradability assessments and testing protocols for WSPs.

Materials and Methods

Software declaration. All simulations, data analysis, and plotting were conducted using R (version 4.4.0) via RStudio (version 2024.0X).

Kinetic Calculation of PEG reaction with •OH. Reaction of PEGs with hydroxyl radical (•OH) was modelled assuming pseudo-first-order reaction kinetics (**Equation 1**) at three steady-state •OH concentrations (i.e., $[\bullet OH]_{SS} = 10^{-15}$ M, 10^{-16} M, and 10^{-17} M) that cover the concentration range reported for sunlit surface waters.[26,28]

$$k_1 = k_M \cdot [\cdot OH]_{SS} \qquad \textbf{Eq. 1}$$

where k_1 (s^{-1}) is the pseudo-first-order reaction rate constant, and k_M (= $2.1 \cdot 10^9$ M^{-1} s^{-1}) is the previously-reported, experimentally-determined rate constant for reaction of •OH with a monomeric unit in dissolved PEG.[43]

The reactions following •OH attack (i.e., addition of dioxygen and intermolecular rearrangements leading to a chain scission) have reported rate constants that are higher than k_1.[33] The overall scission reaction rate, therefore, is close to being diffusion limited (since k_{diff} is usually around 10^{-9}-10^{-10} M^{-1} s^{-1} according to the Smoluchowsky equation). The average scissions per initial polymer (i.e., PEG) chains (hereafter abbreviated by the dimensionless (i.e., number of cuts per one chain) variable $\overline{SiC}(t)$) were derived assuming that all monomeric units of a given PEG molecule have the same probability of reacting with •OH independently of the position of the monomeric units in the chain (**Equation 2**):

$$\overline{SiC}(t) = \frac{\left(1-e^{-k_1 \cdot t}\right) \cdot M_n(t=0)}{MW_{Monomer}} \qquad \textbf{Eq. 2}$$

where t (s) is the reaction time, $\overline{M_n}(t_0)$ is the initial number averaged MW of the ensemble of PEG molecules and $MW_{Monomer}$ is the molecular weight of the monomeric unit (i.e., 44 Da for PEG). The $\overline{SiC}(t)$ were converted into time-dependent, number averaged molecular weights, $\bar{M}_n(t)$, using **Equation 3**:

$$\bar{M}_n(t) = \frac{\overline{M_n}(t_0)}{\overline{SiC}(t)+1} \qquad \textbf{Eq. 3}$$

Equation 3 has been experimentally validated and is widely used to describe polymer chain scissions.[39,44,45]

Molecular weight-dependence of the reaction rate constant for PEG and •OH in Monte Carlo simulations. Reaction rate constants between PEG molecules and •OH depend on the chain length of PEG molecules (i.e., number of repeating monomeric units n) with two distinct kinetic regimes:[46] the reaction-limited regime for small PEG molecules ($n \leq 30$) and the diffusion-limited regime for large PEG molecules ($n > 30$). The transition between the reaction-limited regime for small PEG molecules and the diffusion-limited regime for large PEG molecules is expected to occur around $n = 30$.[46]

In the reaction-limited regime, the reaction rate constant, k_P, of a given PEG molecule is directly proportional to its number of repeating monomeric units n (**Equation 4**):

$$k_P(n) = 0.8 \cdot k_M \cdot n, \qquad \text{for } 1 \leq n \leq 30 \qquad \textbf{Eq. 4}$$

where k_P (M^{-1} s^{-1}) is the rate constant for PEG reacting with •OH. The proportionality constant of 0.8 was selected for PEGs as it was previously reported for the reaction between benzophenone radicals and n-alkanes of various lengths.[47]

Around n > 30 approaching diffusion-limitation of the reaction results from the increased number of reaction sites per PEG molecule, which increases the effective rate constant k_P. At the same time, the larger PEG molecules undergo coiling in solution. Such coiling lowers the rate constant of the reaction between •OH and a monomeric unit of the PEG chain, k_M, because the reaction is preferably occurring on the surface of the PEG coil. This effect can be accounted for by incorporating the effective reaction radius of the PEG molecule into the reaction rate constant using the Smoluchowski equation for diffusion-limited reactions in dilute solutions (**Equation 5**):[46]

$$k_P(n) = 4\pi(R_{\cdot OH} + R_{PEG}) \cdot (D_{\cdot OH} + D_{PEG}) \cdot N_A = 4\pi(R_{\cdot OH} + R_{PEG}) \cdot \left(\frac{k_B T}{6\pi\eta R_{\cdot OH}} + \frac{k_B T}{6\pi\eta R_{PEG}}\right) \cdot N_A, \text{ for } n > 30 \quad \textbf{Eq. 5}$$

where $R_{\cdot OH}$ and R_{PEG} (dm) are the hydrodynamic radii of •OH and the coiled PEG molecule, respectively, T [K] is the temperature, η (kg dm^{-1} s^{-1}) is the dynamic viscosity of water, N_A (mol^{-1}) is the Avogadro constant, and $D_{\cdot OH}$ and D_{PEG} (dm^2 s^{-1}) are the effective diffusion coefficients of the •OH and the PEG molecule, respectively. Since $R_{\cdot OH} << R_{PEG}$ and $D_{\cdot OH} >> D_{PEG}$, equation 5 simplifies to **Equation 6**:

$$k_p(n) = 4\pi \cdot R_{PEG} \cdot D_{\cdot OH} \cdot N_A, \quad \text{for } n > 30 \quad \textbf{Eq. 6}$$

The hydrodynamic radius of the coiled PEG chain, $\boldsymbol{R_{PEG}}$, scales in the Flory theory for good solvents as $\boldsymbol{R_{PEG}} \propto n^{0.6}$. Experimental observations found $\boldsymbol{k_p}(n) \propto n^{0.56}$, for $n > 30$ for PEGs, which is subsequently used as constant parameter for the MW-dependent rate constants in the diffusion-limited regime.[46] The resulting reaction rate constants for the polymer, k_p, and monomeric units, k_M, versus n are plotted in section **S1** of the Supplementary Information (SI)).

Probabilistic simulation of the chain cleavage. The Monte Carlo simulation started by defining the initial chain length distribution of the PEG molecules. The chain lengths, n_i for i = 1, 2, 3, …, m (where m = number of chains with n_i monomeric units), were assumed to follow a normal distribution with a mean chain length λ (representing the average degree of polymerization $\overline{X_n}$), and a standard deviation σ.

Chain-scissions in the simulation was restricted to chains with more than one monomeric unit ($n_i > 1$). For each selected chain with length n_j , a reaction and thus cutting point c_j (where $c_j \in$ (n_j -1) cutting positions) was randomly identified in the simulation. The probability of c_j to be chosen was uniformly distributed between 1 and n_j -1, ensuring that the scission produces two new viable segments (i.e., reaction products). The lengths of these reaction products were n_c and n_j-n_c. The probability of chain j with length n_j to be chosen for scission, $P(n_j)$, is proportional to the continuous rate constant k_p for reaction of PEG and · OH and thus depends on the number of repeating monomeric units n as rationalized above, and thus defined as (**Equation 7**):

$$P(n_j) = \frac{k_P(n_j)}{\sum_{i=1}^{i=m} k_P(n_i)} \qquad \textbf{Eq. 7}$$

$$\text{where } k_P(n_j) = \begin{cases} 0.8 \cdot k_M \cdot n_j & \text{for } n_j \leq 30 \\ 0.8 \cdot k_M \cdot 30 \cdot \left(\frac{n_j}{30}\right)^{0.57} & \text{for } n_j > 30 \end{cases}$$

After each scission, the collection of chains in the simulation is updated by removing the chain with length n_j that reacted and adding the two formed segments with lengths n_c and n_j-n_c. The MW of each chain is calculated by multiplying the number of monomeric units per chain n with the MW of the monomeric unit ($MW_{\text{monomer, 12C-PEG}}$ = 44 Da, $MW_{\text{monomer, 13C-PEG}}$ = 46 Da).

Photodegradation experiments. Solutions of ^{13}C-PEG (Polymer Source Inc., M_n = 6200 Da, M_w/M_n = 1.08; dissolved in MilliQ water to a concentration of 5 mg ^{13}C-PEG ml^{-1} in stock solution) were irradiated in glass tubes in a LZC photoreactor (LZC-4V) equipped with twelve 365 nm UVA broad band bulbs. For each reaction timepoint (t_0= 0 min (unreacted solution), t_1 = 15 min, t_2 = 30 min, and t_3 = 45 min), triplicate solutions were prepared by mixing 6 mL of the above ^{13}C-PEG solution and 2 ml of a 100 mM H_2O_2-solution (prepared in Milli-Q water) in tubes that were placed on a carousel inside the photoreactor. After the respective reaction time, the triplicate tubes were removed from the reactor and the solution in each tube was split into three subsamples: 100 µL were taken for high pressure liquid chromatography with charged aerosol detection and high-resolution mass spectrometry (HPLC-CAD-HR-MS) analysis, 900 µL were taken for ^{13}C-NMR analysis, and 7 mL for the biodegradability testing. Details on the analytical methods are provided in section **S2** (Supplementary Information). At concentrations below 1 mg PEG mL^{-1}, the response of the CAD is independent of PEG MW,[48] allowing for quantification of all molecules of a given *n*. We additionally ran control samples of PEGs (+ H_2O_2) in the dark. These dark controls confirmed that PEGs did not degrade in the absence of light, confirming that the PEG breakdown into lower MW components was caused by •OH photochemically produced from irradiation of the H_2O_2 solution.

Sediment and soil incubations. *Preparations.* Prior to transferring the ^{13}C-PEG solutions (t_0 to t_3) into the incubation bottles, residual H_2O_2 from the solutions was removed by adding 0.05 mL of catalase from bovine liver (Sigma Aldrich, aqueous suspension, $1 \cdot 10^4$ to $4 \cdot 10^4$ units mg^{-1} protein, 0.44 mg protein mL^{-1}) to the 7 mL PEG solution, followed by gentle stirring for 10 minutes. The same amount of catalase in 7 mL of H_2O2 solution without ^{13}C-PEG, was added to the background incubations, to account for any effects on the background mineralization.

The sediment was preincubated for 7 days. Afterwards, each of the reacted PEG solution timepoints was divided in three parts and pipetted into the triplicate sediment incubations with sediment from a sediment core collected in Lake Rotsee in Lucerne, Switzerland (sampling date: 27th September, 2023). The top 5 cm of the sediment core was was mixed with an equal volume of lake water under stirring for 1 h. A volume of 40 mL of the suspension (with approx. 3 g of dry weight of sediment) was transferred into 100 mL Schott bottles used for the incubations (total number of 12). Each bottle was placed in an incubation chamber at 20 °C and continuously stirred over the course of the incubation.

A soil of the Landwirtschaftliche Untersuchungs- und Forschungsanstalt Speyer (LUFA, Germany, 6S soil collected in October 2023; 2 mm sieved) was used for the soil incubations. The soil moisture was adjusted with Milli-Q water to 50% of the maximum water holding capacity (41.4 wt%). Details on soil properties are provided in section S3 (Supplementary Information). The incubation bottles contained 20 g of dry soil + added water, and were run in triplicates.

After preparation of the sediment and the soil, 7 ml of the respective PEG solution (t0 to t3) were added dropwise to the incubation bottle. The samples were subsequently incubated for 150 days at 20 °C. The water mass was determined gravimetrically and adjusted biweekly (after the first 4 weeks of incubation).

Quantification of PEG-derived $^{13}CO_2$ formed in incubations. The mineralization of ^{13}C-labelled PEGs to $^{13}CO_2$ was followed in triplicate incubation bottles. The bottles were placed in an incubation system with automated gas phase $^{13}CO_2$ analysis, as previously described.[36] Modifications of the incubation setup (e.g., using pressurized air in the inlet) used in this study are described in section **S4** (Supplementary Information).

Closing mass balances on added PEG carbon-13. After terminating the sediment and soil incubations, we determined the non-mineralized residual PEG-added carbon-13, $^{13}C_{Non-}$

$_{Mineralized}$, in each incubation bottle. While $^{13}C_{Non\text{-}Mineralized}$ can be present either as biomass formed during metabolic utilization of the PEG or residual polymeric PEG (either in the form of the original PEG or partially biodegraded molecules), these two pools were quantified only in their total sum. To this end, the sediment or soil from each incubation flask was first freeze-dried and subsequently milled (frequency of 30 Hz for 1 min in a MM400 oscillatory ball mill from Retsch GmbH & Co). An aliquot of 10 mg was then subsampled from each milled sediment and soil for elemental analysis (EA) coupled to isotope ratio mass spectrometry (IRMS) to quantify $^{13}C_{Non\text{-}Mineralized}$, as described previously.[36] Details on the analyses are provided in section **S5** (Supplementary Information).

Acknowledgments

We thank Prof. Dr. Carsten Schubert (Eawag) for sampling and providing the Rotsee sediment and Prof. Dr. Lenny Winkel (ETHZ and Eawag) for access to and support on the Orbitrap Mass Spectrometer. M.S. acknowledges funding from the Joint Research Network on Advanced Materials and Systems (JONAS) program of BASF SE and ETH Zurich. M.S. and K.K. thank Dr. Rupert Konradi (Director of JONAS) for scientific input.

Author Contributions

K.K. and M.S. conceptualized the study, interpreted the data, and wrote the manuscript. K.K. performed all modelling, experimental work, drafted the manuscript. M.J. and S.M.B. contributed to the elemental analysis-isotope ratio mass spectrometry (EA-IRMS). R.A.S. assisted in the setup of incubations, and C.S. provided support for high-performance liquid chromatography anaysis coupled to charged aerosol detection and mass spectrometry (HPLC-CAD-MS). K.M. contributed to the conceptualization of the photochemical model. M.S. secured funding. All authors reviewed and revised the manuscript.

Competing interests

M.S. received funding through the Joint Research Network on Advanced Materials and Systems (JONAS), a collaborative initiative between BASF SE and ETH Zurich. G.B. and A.K. are employed by BASF SE, which manufactures and commercializes conventional and biodegradable polymers. Furthermore, G.B. and A.K. contribute as industrial experts to multiple associations focused on biodegradable and compostable polymers.

Data availabillity

The data presented as well as the numerical model are available at the ETH Zurich Research Collection (https://doi.org/10.3929/ethz-b-000717692).

References

1. Hoffmann, M. M. Polyethylene glycol as a green chemical solvent. *Current Opinion in Colloid & Interface Science* **57**, 101537 (2022).
2. Jang, H.-J., Shin, C. Y. & Kim, K.-B. Safety Evaluation of Polyethylene Glycol (PEG) Compounds for Cosmetic Use. *Toxicological Research* **31**, 105–136 (2015).
3. Gaballa, S., Naguib, Y., Mady, F. & Khaled, K. Polyethylene glycol: Properties, applications, and challenges. *Journal of advanced Biomedical and Pharmaceutical Sciences* **0**, 26–36 (2023).
4. Kleemann, K. & Sander, M. Water-soluble and Water-dispersible Polymers Used in Commercial Agricultural Formulations: Inventory of Polymers and Perspective on their Environmental Fate. *Chimia* **77**, 764–772 (2023).
5. Szymanski, A., Wyrwas, B. & Lukaszewski, Z. Determination of non-ionic surfactants and their biotransformation by-products adsorbed on alive activated sludge. *Water Research* **37**, 281–288 (2003).
6. Huppertsberg, S., Zahn, D., Pauelsen, F., Reemtsma, T. & Knepper, T. P. Making waves: Water-soluble polymers in the aquatic environment: An overlooked class of synthetic polymers? *Water Research* **181**, 115931 (2020).
7. Arp, H. P. H. & Knutsen, H. Could We Spare a Moment of the Spotlight for Persistent, Water-Soluble Polymers? *Environ. Sci. Technol.* **54**, 3–5 (2020).

8. Kleemann, K. *et al.* Molecular Structure and Conformation of Biodegradable Water-Soluble Polymers Control Adsorption and Transport in Model Soil Mineral Systems. *Environ. Sci. Technol.* **58**, 1274–1286 (2024).
9. Castanho, G. M., Regitano, J. B., Tornisielo, V. L. & Abdalla, A. L. Sorption and mobility of polyethylene glycol (PEG 4000) in tropical soils. *Toxicological & Environmental Chemistry* **91**, 1263–1271 (2009).
10. Kawai, F. & Yamanaka, H. Biodegradation of polyethylene glycol by symbiotic mixed culture (obligate mutualism). *Arch. Microbiol.* **146**, 125–129 (1986).
11. Kawai, F. Microbial degradation of polyethers. *Applied Microbiology and Biotechnology* **58**, 30–38 (2002).
12. Kawai, F. *et al.* Bacterial oxidation of polyethylene glycol. *Appl Environ Microbiol* **35**, 679–684 (1978).
13. Sugimoto, M. *et al.* The First Step in Polyethylene Glycol Degradation by Sphingomonads Proceeds via a Flavoprotein Alcohol Dehydrogenase Containing Flavin Adenine Dinucleotide. *J Bacteriol* **183**, 6694–6698 (2001).
14. Tachibana, S., Kuba, N., Kawai, F., Duine, J. A. & Yasuda, M. Involvement of a quinoprotein (PQQ-containing) alcohol dehydrogenase in the degradation of polypropylene glycols by the bacterium *Stenotrophomonas maltophilia*. *FEMS Microbiology Letters* **218**, 345–349 (2003).
15. Nascimento, Í. F. *et al.* Polyethylene glycol acute and sub-lethal toxicity in neotropical Physalaemus cuvieri tadpoles (Anura, Leptodactylidae). *Environmental Pollution* **283**, 117054 (2021).
16. Hatami, M., Banaee, M. & Nematdoost Haghi, B. Sub-lethal toxicity of chlorpyrifos alone and in combination with polyethylene glycol to common carp (Cyprinus carpio). *Chemosphere* **219**, 981–988 (2019).

17. Nigro, L. *et al.* Unveiling the multilevel impact of four water-soluble polymers on Daphnia magna: From proteome to behaviour (a case study). *Journal of Hazardous Materials* **469**, 134000 (2024).
18. Zicarelli, G. *et al.* Toxicity of water-soluble polymers polyethylene glycol and polyvinyl alcohol for fish and frog embryos. *Science of The Total Environment* **933**, 173154 (2024).
19. Hisar, O. & Oehlmann, J. Individual and combined ecotoxic effects of water-soluble polymers. *PeerJ* **11**, e16475 (2023).
20. Duis, K., Junker, T. & Coors, A. Environmental fate and effects of water-soluble synthetic organic polymers used in cosmetic products. *Environ Sci Eur* **33**, 21 (2021).
21. Wang, T. *et al.* Impact of molecular weight on the mechanism of cellular uptake of polyethylene glycols (PEGs) with particular reference to P-glycoprotein. *Acta Pharmaceutica Sinica B* **10**, 2002–2009 (2020).
22. Bernhard, M., Eubeler, J. P., Zok, S. & Knepper, T. P. Aerobic biodegradation of polyethylene glycols of different molecular weights in wastewater and seawater. *Water Research* **42**, 4791–4801 (2008).
23. McLaughlin, M. C., Borch, T. & Blotevogel, J. Spills of Hydraulic Fracturing Chemicals on Agricultural Topsoil: Biodegradation, Sorption, and Co-contaminant Interactions. *Environ. Sci. Technol.* **50**, 6071–6078 (2016).
24. Abdalla, A. L. *et al.* Biodegradation of polyethylene glycol (PEG) in three tropical soils using radio labelled PEG. *Animal Feed Science and Technology* **122**, 187–193 (2005).
25. Gligorovski, S., Strekowski, R., Barbati, S. & Vione, D. Environmental Implications of Hydroxyl Radicals ($^{\bullet}$OH). *Chem. Rev.* **115**, 13051–13092 (2015).
26. Brezonik, P. L. & Fulkerson-Brekken, J. Nitrate-Induced Photolysis in Natural Waters: Controls on Concentrations of Hydroxyl Radical Photo-Intermediates by Natural Scavenging Agents. *Environ. Sci. Technol.* **32**, 3004–3010 (1998).

27. Zepp, R. G., Hoigne, Juerg. & Bader, Heinz. Nitrate-induced photooxidation of trace organic chemicals in water. *Environ. Sci. Technol.* **21**, 443–450 (1987).

28. Haag, W. R. & Hoigné, J. Photo-sensitized oxidation in natural water via .OH radicals. *Chemosphere* **14**, 1659–1671 (1985).

29. Russi, H., Kotzias, D. & Korte, F. Photoinduzierte hydroxylierungsreaktionen organischer chemikalien in natürlichen Gewässern - Nitrate als potentielle OH-radikalquellen -. *Chemosphere* **11**, 1041–1048 (1982).

30. Vione, D. *et al.* Sources and Sinks of Hydroxyl Radicals upon Irradiation of Natural Water Samples. *Environ. Sci. Technol.* **40**, 3775–3781 (2006).

31. White, E. M., Vaughan, P. P. & Zepp, R. G. Role of the photo-Fenton reaction in the production of hydroxyl radicals and photobleaching of colored dissolved organic matter in a coastal river of the southeastern United States. *Aquatic Sciences - Research Across Boundaries* **65**, 402–414 (2003).

32. Lam, M. W., Tantuco, K. & Mabury, S. A. PhotoFate: A New Approach in Accounting for the Contribution of Indirect Photolysis of Pesticides and Pharmaceuticals in Surface Waters. *Environ. Sci. Technol.* **37**, 899–907 (2003).

33. Guo, X., Minakata, D. & Crittenden, J. Computer-Based First-Principles Kinetic Monte Carlo Simulation of Polyethylene Glycol Degradation in Aqueous Phase UV/H_2O_2 Advanced Oxidation Process. *Environ. Sci. Technol.* **48**, 10813–10820 (2014).

34. Santos, L. C., Poli, A. L., Cavalheiro, C. C. S. & Neumann, M. G. The UV/H2O2 - photodegradation of poly(ethyleneglycol) and model compounds. *J. Braz. Chem. Soc.* **20**, 1467–1472 (2009).

35. Zumstein, M. T. *et al.* Biodegradation of synthetic polymers in soils: Tracking carbon into CO_2 and microbial biomass. *Sci. Adv.* **4**, eaas9024 (2018).

36. Nelson, T. F. *et al.* Biodegradation of poly(butylene succinate) in soil laboratory incubations assessed by stable carbon isotope labelling. *Nat Commun* **13**, 5691 (2022).

37. Batiste, D. C. *et al.* Site-Specific Mineralization of a Polyester Hydrolysis Product in Natural Soil. *ACS Sustainable Chem. Eng.* **10**, 1373–1378 (2022).

38. Sander, M., Kohler, H.-P. E. & McNeill, K. Assessing the environmental transformation of nanoplastic through 13C-labelled polymers. *Nat. Nanotechnol.* **14**, 301–303 (2019).

39. Santos, L. C., Poli, A. L., Cavalheiro, C. C. S. & Neumann, M. G. The UV/H2O2 - photodegradation of poly(ethyleneglycol) and model compounds. *J. Braz. Chem. Soc.* **20**, 1467–1472 (2009).

40. Payne, M. E., Kareem, O. O., Williams-Pavlantos, K., Wesdemiotis, C. & Grayson, S. M. Mass spectrometry investigation into the oxidative degradation of poly(ethylene glycol). *Polymer Degradation and Stability* **183**, 109388 (2021).

41. Sinsabaugh, R. L. *et al.* Stoichiometry of microbial carbon use efficiency in soils. *Ecological Monographs* **86**, 172–189 (2016).

42. Pinot, M. *et al.* Polyunsaturated phospholipids facilitate membrane deformation and fission by endocytic proteins. *Science* **345**, 693–697 (2014).

43. Minakata, D., Li, K., Westerhoff, P. & Crittenden, J. Development of a Group Contribution Method To Predict Aqueous Phase Hydroxyl Radical (HO•) Reaction Rate Constants. *Environ. Sci. Technol.* **43**, 6220–6227 (2009).

44. Rabek, J. F. *Photodegradation of Polymers: Physical Characteristics and Applications*. (Springer, Berlin ; New York, 1996).

45. Hoekstra, H. D., Spoormaker, J. L., Breen, J., Audouin, L. & Verdu, J. UV-exposure of stabilized and non-stabilized HDPE films: physico-chemical characterization. *Polymer Degradation and Stability* **49**, 251–262 (1995).

46. Matheson, M. S., Mamou, A., Silverman, J. & Rabani, J. Reaction of hydroxyl radicals with polyethylene oxide in aqueous solution. *J. Phys. Chem.* **77**, 2420–2424 (1973).
47. Winnik, M. A. & Maharaj, U. Photoreaction of Benzophenone with the n-Alkanes: A Model for Biomolecular Reactions of Polymers. *Macromolecules* **12**, 902–905 (1979).
48. Wang, J., Tang, S. & Zhang, K. Quantitation of polyethylene glycol by size exclusion chromatography with charged aerosol, differential refractive index, and multi-angle light scattering detectors. *Journal of Pharmaceutical and Biomedical Analysis* **238**, 115854 (2024).